Schiff Bases Functionalized With T-Butyl Groups As Adequate Ligands to Extended Assembly of Cu(II) Helicates

Sandra Fernández-Fariña *, Isabel Velo-Heleno, Miguel Martínez-Calvo, Marcelino Maneiro, Francisco Rivadulla, Rosa Pedrido *, Ana M. González-Noya

Posted Date: 28 April 2023

doi: 10.20944/preprints202304.1135.v1

Keywords: Schiff bases; copper; helicates; magnetic properties

Article

Schiff Bases Functionalized with t-Butyl Groups as Adequate Ligands to Extended Assembly of Cu(II) Helicates

Sandra Fernández-Fariña [1,*], Isabel Velo-Heleno [1], Miguel Martínez-Calvo [1], Marcelino Maneiro [2], Francisco Rivadulla [3], Rosa Pedrido [1,*] and and na M. González-Noya [1]

[1] Departamento de Química Inorgánica, Facultade de Química, Campus Vida, Universidade de Santiago de Compostela, 15782 Santiago de Compostela, Spain
[2] Departamento de Química Inorgánica, Facultade de Ciencias, Universidade de Santiago de Compostela, 27002 Lugo, Spain
[3] CIQUS, Centro Singular de Investigación en Química Biolóxica e Materiais Moleculares, Departamento de Química-Física, Universidade de Santiago de Compostela, 15782-Santiago de Compostela, Spain
* Correspondence: sandra.fernandez.farina@usc.es (S.F.-F), rosa.pedrido@usc.es (R.P.)

Abstract. The study of the inherent factors that influence the isolation of one type of metallosupramolecular architecture over another is one of the main objectives in the field of Metallosupramolecular Chemistry. In this work, we report two new neutral copper(II) helicates, $[Cu_2(L^1)_2]\cdot 4CH_3CN$ and $[Cu_2(L^2)_2]\cdot CH_3CN$, obtained by means of an electrochemical methodology and derived from two Schiff-based strands functionalized with ortho-and para-t-butyl groups on the aromatic surface. These small modifications let us to explore the relationship between the ligand design and the structure of the extended metallosupramolecular architecture. The magnetic properties of the Cu(II) helicates were explored by EPR spectroscopy and DC magnetic susceptibility measurements.

Keywords: Schiff bases; copper; helicates; magnetic properties

1. Introduction

The search for new routes to obtain new metallosupramolecular architectures and the study of their potential applications is a field of great interest in Metallosupramolecular Chemistry. The knowledge of the different factors that influence the self-assembly process is essential to control the obtainment of a specific type of compound, so it is necessary to deepen our understanding by designing new systems. Among all factors, the ligand design directly influences the structure of the final metallosupramolecular architecture and thus in its properties and applications [1].

The term "helicate" was introduced by Jean-Marie Lehn in 1987 to describe a class of copper(I) compounds exhibiting a helicoidal architecture with similar characteristics to the DNA double helix [2]. A helicate consists of one or more organic ligands that wrap helically around a series of metal ions that define the helix axis [3].

To obtain helicoidal architectures, the precursor ligands should contain two or more binding domains separated by a flexible spacer to allow helical coiling, but also it should be rigid enough to prevent multiple binding domains coordinating to the same metal ion, giving rise to mononuclear species [4–6]. Moreover, it was demonstrated that the isolation of helicoidal architectures over other possible arrangements can be controlled by the intra- and intermolecular interactions established by the ligand units [7,8]. In the literature there is a large variety of examples of helicate-type extended architectures whose formation is favored and determined by the existence of weak non-covalent π-π or CH···π interactions [4,9].

Nowadays the research on metal helicates is mainly directed towards the search of their potential applications [10–13]. Between these properties there is a special interest on those helicates exhibiting a relevant magnetic behaviour that could be used as new magnetic materials [14–16].

Preprints (www.preprints.org) | NOT PEER-REVIEWED | Posted: 28 April 2023 doi:10.20944/preprints202304.1135.v1

However, the factors that selectively lead to a particular type of metallosupramolecular compound, and to helicates in particular, continues to be of interest and deserve to be further investigated.

Schiff base ligands have been extensively used in Coordination Chemistry [17–19] and more particularly in Metallosupramolecular Chemistry to obtain helicates [11,20], showing some of them relevant biomedical [20] or photophysical [11] properties. In this context, this type of ligands were employed by our research group to obtain the first example of a network assembled from Cu(II) helicates through intermolecular π-π interactions showing an antiferromagnetic behavior [22]. In this primary work the antiferromagnetic character was attributed to the establishment of weak π-π interactions between neighboring helicate units.

With this precedent in mind, in an attempt to explore the relationship between the ligand design, the extended helical structure and the magnetic properties, we will approach the obtainment of helicates combining Schiff base ligands, copper(II) ions and an electrochemical methodology. Herein, we report two novel copper(II) helicates derived from two Schiff base ligands substituted in with t-butyl groups and their crystal structures. We have studied their magnetic properties by EPR spectroscopy and DC magnetic susceptibility.

2. Results and Discussion

2.1. Synthesis and characterization of the ligands H_2L^1 and H_2L^2

In the present work, we will approach the obtainment of extended helicates using dianiline-derived Schiff base ligands. It should be highlighted that the long and semi-flexible dianiline-type spacers have been widely used by Hannon and co-workers, proving to be an effective unit for obtaining a wide variety of helicoidal architectures using different metal ions [23–25]. For this purpose, we have designed two new Schiff base ligands containing the dianiline spacer and two terminal hydroxybenzaldehyde rings decorated with *ortho* and *para* tert-butyl groups (H_2L^1 and H_2L^2, Scheme 1).

The ligands H_2L^1 and H_2L^2 are potentially dianionic with two bidentate [NO] domains separated by a semi-flexible aromatic spacer, factors that should favor the isolation of helical-type complexes. The main objective is to find out whether the position of the tert-butyl group influences the final discrete and extended architecture and the magnetic properties of the final compounds.

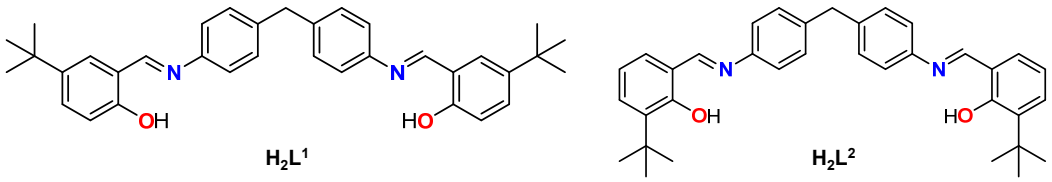

Scheme 1. Schiff base ligands H_2L^1 and H_2L^2.

Both ligands have been synthesized by reaction between the corresponding hydroxybenzaldehyde functionalized with tert-butyl groups and 4,4'-methylenedianiline in 2:1 ratio, using absolute ethanol as solvent (Scheme 2). H_2L^1 and H_2L^2 have been fully characterized by melting point determination, elemental analysis, infrared spectroscopy, mass spectrometry and ^1H NMR spectroscopy techniques (Figures S1 and S2, Supplementary Material).

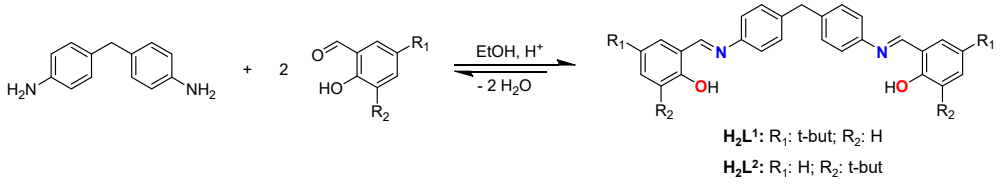

Scheme 2. Synthesis of the Schiff base ligands H_2L^1 and H_2L^2.

2.2. Synthesis and characterization of the copper complexes

Preprints (www.preprints.org) | NOT PEER-REVIEWED | Posted: 28 April 2023 doi:10.20944/preprints202304.1135.v1

Two neutral copper complexes were isolated from H_2L^1 and H_2L^2 using an electrochemical methodology (details in Experimental section). The electrochemical synthesis of the neutral metal complexes was carried out by oxidation of a copper plate in a conductive solution of the corresponding ligand in acetonitrile. The efficiency values calculated, for the electrochemical synthesis of both complexes have values around 0.5 mol·F^{-1}, so the proposed mechanism would involve the loss of two electrons for each metal atom, as shown below:

$$\text{Cathode: } 2\ H_2L^{1|2} + 4\ e^- \rightarrow 2\ (L^{1|2})^{2-} + 2\ H_2(g)$$

$$\text{Anode: } 2\ Cu \rightarrow 2\ Cu^{2+} + 4\ e^-$$

$$\text{Global: } 2\ (L^{1|2})^{2-} + 2\ Cu^{2+} \rightarrow Cu_2(L^{1|2})_2$$

The resulting brown solid complexes were characterized by melting point determination, elemental analysis, infrared spectroscopy, X-ray diffraction and mass spectrometry (Figures S3–S5, Supplementary Material).

Both analytical and spectroscopic data allow us to propose dinuclear stoichiometries of the type $[Cu_2(L^{1|2})_2]$, being the ligands coordinated to the copper centers in their dianionic form $[L^{1|2}]^{2-}$. The infrared spectra of both complexes exhibit a slight shift of the characteristic bands of the ligand skeletons to lower wavenumbers due to the coordination of the metal ions. More in detail, a variation in the ν(C=N) band is observed, indicating that the ligand is bound to the metal *via* the imine nitrogen atoms. Also, the decrease in intensity and the shift of the vibration band (C-O) suggests the coordination of the copper(II) ions through the phenolic oxygen atoms of the ligand. The formation of the copper(II) complexes derived from the Schiff base ligands H_2L^1 and H_2L^2 was also confirmed by MALDI-TOF (+) mass spectrometry, as the peaks corresponding to the dinuclear fragments $[Cu_2L_2 + H]^+$ are observed in the mass spectra of both complexes.

2.2.1. X-ray structures

Slow evaporation of the mother liquors from the synthesis of $[Cu_2(L^1)_2]$ and $[Cu_2(L^2)_2]\cdot CH_3CN$ complexes allowed us to achieve good-quality crystals for X-ray diffraction studies. The crystal structures of the complexes ($[Cu_2(L^1)_2]\cdot 4CH_3CN$ and $[Cu_2(L^2)_2]\cdot CH_3CN$ are depicted in Figures 1 and 2. Table S1 contains the main crystallographic data for these complexes, whereas Tables S2-S3 summarizes the most relevant distances and angles.

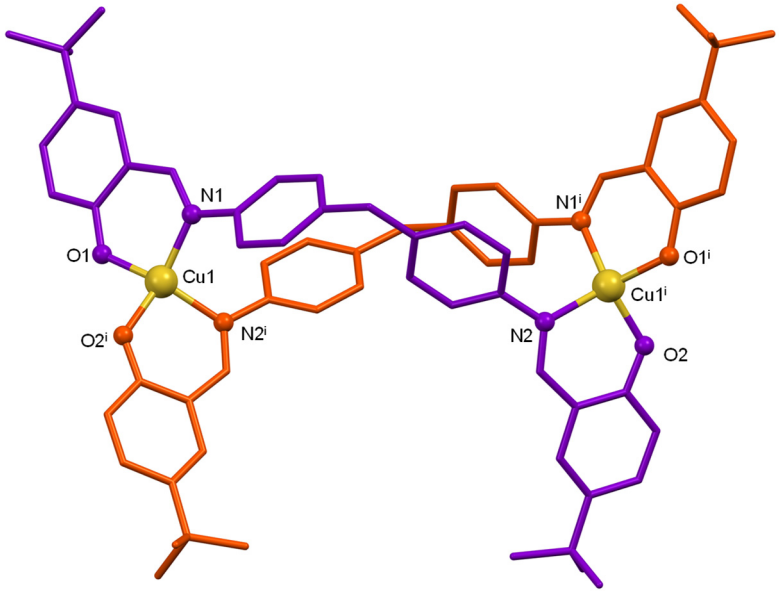

Figure 1. Crystal structure of the copper(II) helicate $[Cu_2(L^1)_2]\cdot 4CH_3CN$. Solvent molecules and hydrogen atoms were omitted for clarity.

Preprints (www.preprints.org) | NOT PEER-REVIEWED | Posted: 28 April 2023 doi:10.20944/preprints202304.1135.v1

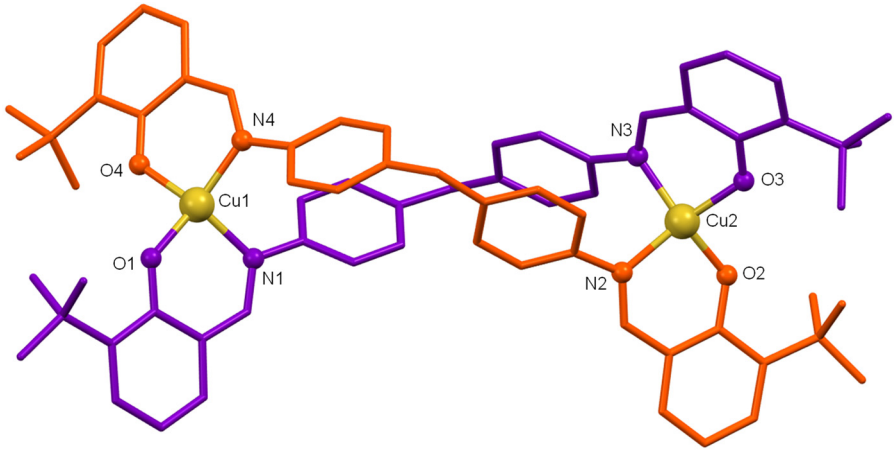

Figure 2. Crystal structure of the copper(II) helicate $[Cu_2(L^2)_2]\cdot CH_3CN$. Solvent molecules and hydrogen atoms were omitted for clarity.

The discrete crystal structures of both compounds are similar so, a joint discussion will be performed, highlighting differences. Both structures show neutral dinuclear helicate-type architectures formed by two strands of bideprotonated ligand $[L^{1|2}]^{2-}$ that cross each other when coordinating the two Cu(II) ions (Figures 1 and 2). The ligands act in such a way that each of their bidentate [NO] branches coordinates to a different metal ion giving rise to a distorted tetrahedral geometry [≠ 109.5º] for the Cu(II) ions. The O-M-N bond angles clearly show the distortion of the tetrahedral geometry (Tables S2-S3).

The main bond distances Cu-O and Cu-N are in the expected ranges for Cu(II) complexes derived from Schiff base ligands with phenol groups [26] with the bond distance Cu-O being slightly smaller than Cu-N (see Tables S2-S3). The intermetallic distance Cu····Cu (11,76 Å for $[Cu_2(L^1)_2]\cdot 4CH_3CN$ and 11,87 Å for $[Cu_2(L^2)_2]\cdot CH_3CN$) are in the order of those found for other Cu(II) helicates with dianiline-type spacers and does not deserve further comments [27].

Each helicate molecule displays eight aromatic rings which makes possible the establishment of aromatic π-π or CH····π stacking interactions. Thus, both copper(II) helicates display weak π-π interactions between the aromatic rings of the two aniline spacers that contribute to the stabilization of the helicoidal structure (distance between centroids: 3.890 Å for $[Cu_2(L^1)_2]\cdot 4CH_3CN$; 3.92 Å and 3.86 Å for $[Cu_2(L^2)_2]\cdot CH_3CN$, Figure 3).

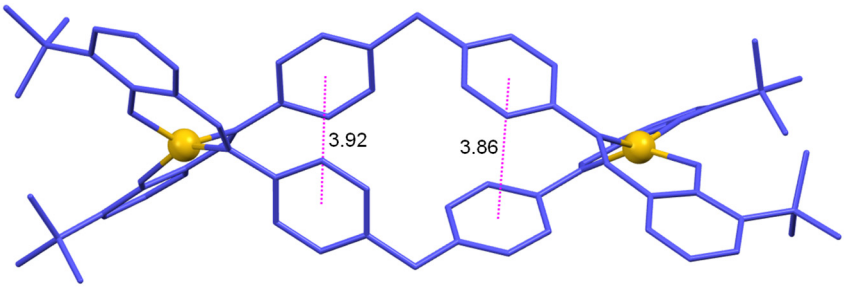

Figure 3. π-π interactions between the aromatic rings of the two ligands in the copper(II) helicate $[Cu_2(L^2)_2]\cdot CH_3CN$.

The crystal lattice of $[Cu_2(L^1)_2]\cdot 4CH_3CN$ (Figure 4) show intermolecular π-π interactions involving the aromatic rings of the spacer of adjacent helicate units (centroid-centroid distance 4.00 Å), being these interactions similar than the intramolecular ones (3.89 Å). These interactions are also observed between one of the phenyl rings of the spacer and the aromatic ring of a linker domain (centroid-centroid distance 4.32 Å (Figure 4). In addition, CH···π interactions between the aromatic ring of one of the ligand branches and one of the tert-butyl substituents of the adjacent helicate can be observed in the $[Cu_2(L^1)_2]\cdot 4CH_3CN$ (3.79 Å) cell, Figure S4, Supplementary Material.

Preprints (www.preprints.org) | NOT PEER-REVIEWED | Posted: 28 April 2023 doi:10.20944/preprints202304.1135.v1

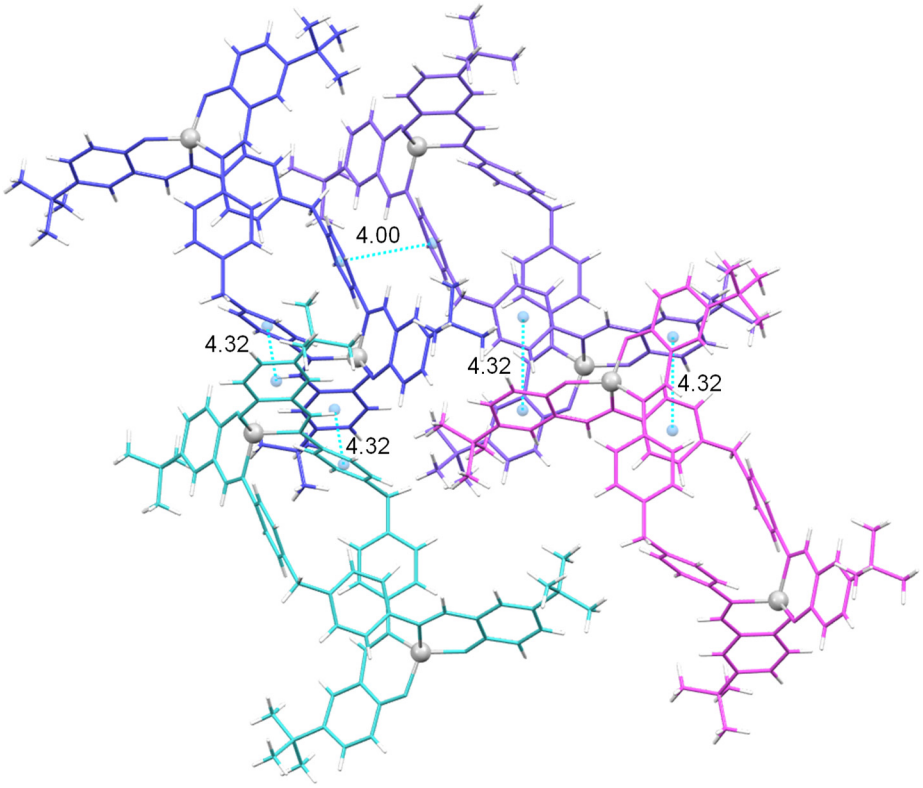

Figure 4. Intermolecular π-stacking interactions in the crystal lattice of the complex $[Cu_2(L^1)_2]\cdot 4CH_3CN$.

It should be note that, the only interaction that can be observed in the crystal lattice of the helicate $[Cu_2(L^2)_2]\cdot CH_3CN$ involves one of the phenyl rings of the spacer and the benzene of a linker domain (centroid-centroid distance 3.79 Å) being an important difference compared to the $[Cu_2(L^1)_2]\cdot 4CH_3CN$ helicate (Figure S5).

In addition, the copper(II) helicate $[Cu_2(L^2)_2]\cdot CH_3CN$, that incorporates the tert-butyl groups adjacent to the phenolic groups, establish hydrogen bonds interactions between the CH_3 of the tert-butyl groups and the phenolic oxygen atoms (Figure 5) [28].

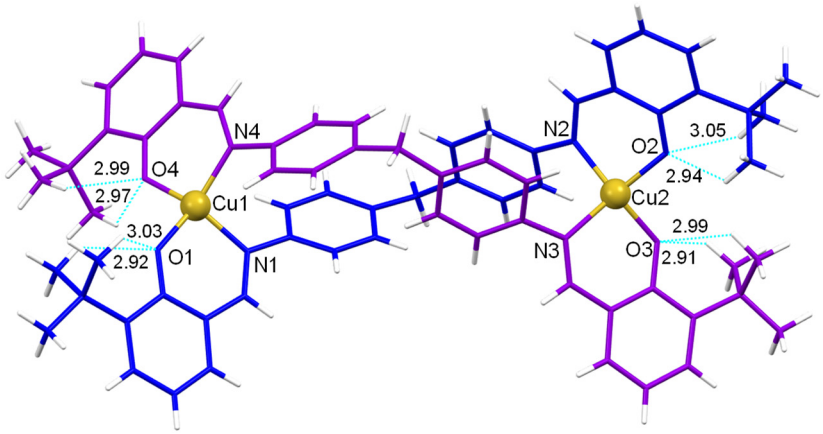

Figure 5. Crystal structure of the $[Cu_2(L^2)_2]\cdot CH_3CN$ helicate showing the intramolecular hydrogen bonds: C29–H29B···O1 2.92 Å, C30–H30C···O1 3.03 Å, C69–H69B···O4 2.97 Å, C70–H70C···O4 2.99 Å, C34–H34C···O2 2.94 Å, C33–H33B···O2 3.05 Å, C64–H64B···O3 2.91 Å, C65–H65C···O3 2.99 Å.

It is remarkable to mention that in the case of the two helicates described in this work the distance between the Cu(II) ions of the closest stacked helicates (intermolecular metal distance) is

Preprints (www.preprints.org) | NOT PEER-REVIEWED | Posted: 28 April 2023 doi:10.20944/preprints202304.1135.v1

notably smaller than the distance between the two metal atoms within the molecule, in the same way as the copper(II) helicate reported by us in 2003 [22] and the cobalt(II) helicate reported later on by Andruh and co-workers [29]. This interesting structural arrangement could affect to the magnetic properties of the two helicates, as discussed below.

It is also worth mentioning that the intermolecular distance between metal ions is smaller in the case of the $[Cu_2(L^1)_2]\cdot 4CH_3CN$ helicate [~5.6 Å] (Figure 6), which exhibit the tert-butyl substituent in *para* position with respect to the phenolic oxygen, compared with that in the $[Cu_2(L^2)_2]\cdot CH_3CN$ helicate, which incorporate the tert-butyl substituent in *ortho* position [~7.1 Å] (Figure 7).

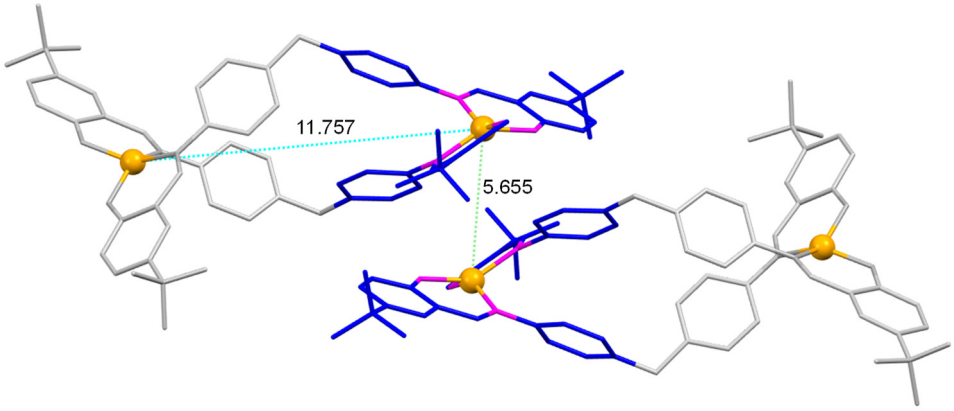

Figure 6. Part of the crystalline cell of the $[Cu_2(L^1)_2]\cdot 4CH_3CN$ helicate, showing the π-π type interactions (rings in blue), as well as the intramolecular (blue) and intermolecular M-M distances with the metal ions of the adjacent ligand (green).

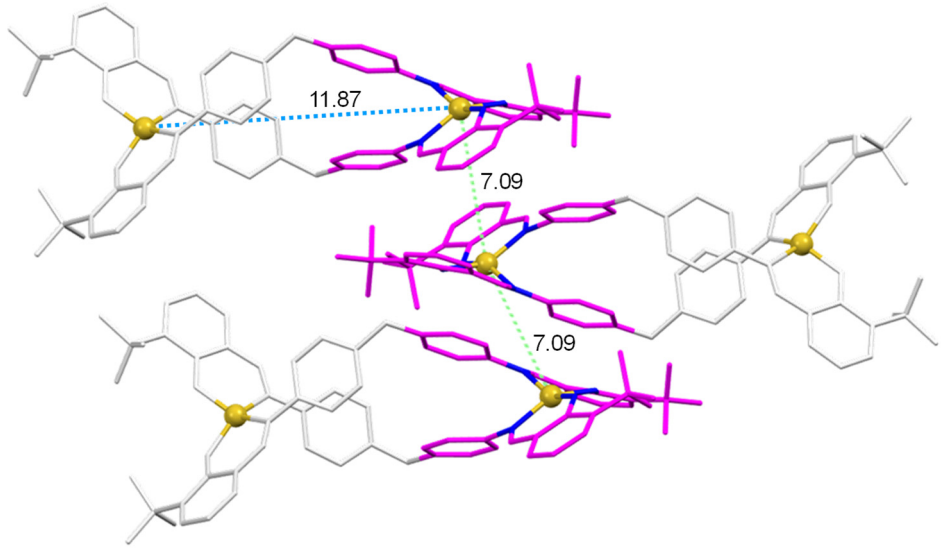

Figure 7. Part of the crystalline cell of the $[Cu_2(L^2)_2]\cdot CH_3CN$ helicate, showing the π-π type interactions (pink rings), as well as the intramolecular (blue) and intermolecular M-M distances with the metal ions of the closest helicates (green).

All the exposed confirms that the highly aromatic Schiff base ligands H_2L^1 and H_2L^2 are suitable to obtain extended helicate structures through weak intermolecular interactions. Besides, the position of the bulky t-butyl groups influences the microarchirecture of the extended structure, as demonstrated by the shorter intermolecular Cu---Cu distance displayed when the ligand exhibits the tert-butyl groups far away from the binding sites (para position).

2.3. Magnetic properties of helicates

Preprints (www.preprints.org) | NOT PEER-REVIEWED | Posted: 28 April 2023 doi:10.20944/preprints202304.1135.v1

It is well known that in coordination compounds metal ions can interact with each other when the distance between them is small [30]. Additionally, in the literature there are examples of helicoidal supramolecular architectures with large intramolecular M-M distances showing relevant magnetic behavior for which interesting nanotechnological applications are proposed. As mentioned above, the origin of this magnetic behavior could be due to the fact that the interhelicoidal M-M distance is fairly small and, therefore, the interaction between metal ions of adjacent molecules takes place [22,29,31].

Thus, taking into account the above background, the magnetic properties of the copper(II) $[Cu_2(L^1)_2]\cdot 4CH_3CN$ and $[Cu_2(L^2)_2]\cdot CH_3CN$ helicates were studied by DC magnetic susceptibility and EPR spectroscopy .

The temperature dependence of the magnetic susceptibility, χ, is shown in Figure 8. At first sight both compounds show a Curie-like behavior, without any hint of magnetic ordering down to 5 K. The two copper complexes show a $\chi_M T \approx 0.7$ emu K mol^{-1} at low temperature, close to $\chi_M T \approx 0.75$ emu K mol^{-1} expected for a molecule with two independent Cu^{2+} ions with spin-only contribution (μ=1.73 μ_B). However, increasing temperature enhances $\chi_M T$ for $[Cu_2(L^1)_2]\cdot 4CH_3CN$, while it decreases slightly in $[Cu_2(L^2)_2]\cdot CH_3CN$.

Considering the total orbital contribution to the magnetic moment in Cu^{2+} ions will result in a μ=3.54 $\mu_{B/Cu}$, and hence $\chi_M T \approx 3.5$ emu K mol^{-1} for a lattice with two Cu sites. In the tetrahedral d^9 configuration, the unpaired electron can occupy the dxz or dyz orbitals, so that the complex acquires an orbital angular momentum. The observed increase of $\chi_M T$ in $[Cu_2(L^1)_2]\cdot 4CH_3CN$ suggests a substantial orbital contribution from a partially distorted octahedral configuration (attributed to acetonitrile coordination), whose orbital occupation changes with temperature.

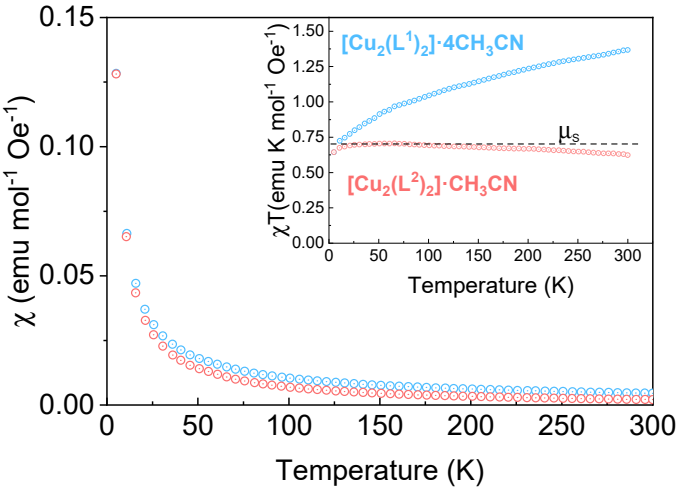

Figure 8. Temperature dependence of the molar magnetic susceptibility, χ, for $[Cu_2(L^1)_2]\cdot 4CH_3CN$ and $[Cu_2(L^2)_2]\cdot CH_3CN$ helicates, measured at H=100 Oe. The inset shows the temperature dependence of χT, proportional to the magnetic moment of the samples.

The differences in the local coordination of copper in both complexes is further demonstrated by the differences observed in the EPR spectra of Cu^{2+} species, shown in Figure 9. The $[Cu_2(L^2)_2]\cdot CH_3CN$ shows the typical EPR spectrum for an axial complex of Cu^{2+} (S=1/2) with $g_{//}(\approx 2.26) > g_{\perp}(\approx 2.08)$. These values are in the range reported for copper tetracoordinated by two oxygen and two nitrogen atoms [N_2O_2] [32,33]. The hyperfine coupling with the copper nucleus (I = 3/2) is not resolved at g//, which could be due to broadening by dipole–dipole interactions.

On the other hand, $[Cu_2(L^1)_2]\cdot 4CH_3CN$ shows a more complex spectrum, consistent with a distorted structure, which could justify a larger and temperature dependent orbital contribution to $\chi_M T$, discussed before. The contribution from two copper sites cannot be discarded, and a complete elucidation of the EPR spectrum of this helicate requires further investigation.

Preprints (www.preprints.org) | NOT PEER-REVIEWED | Posted: 28 April 2023 doi:10.20944/preprints202304.1135.v1

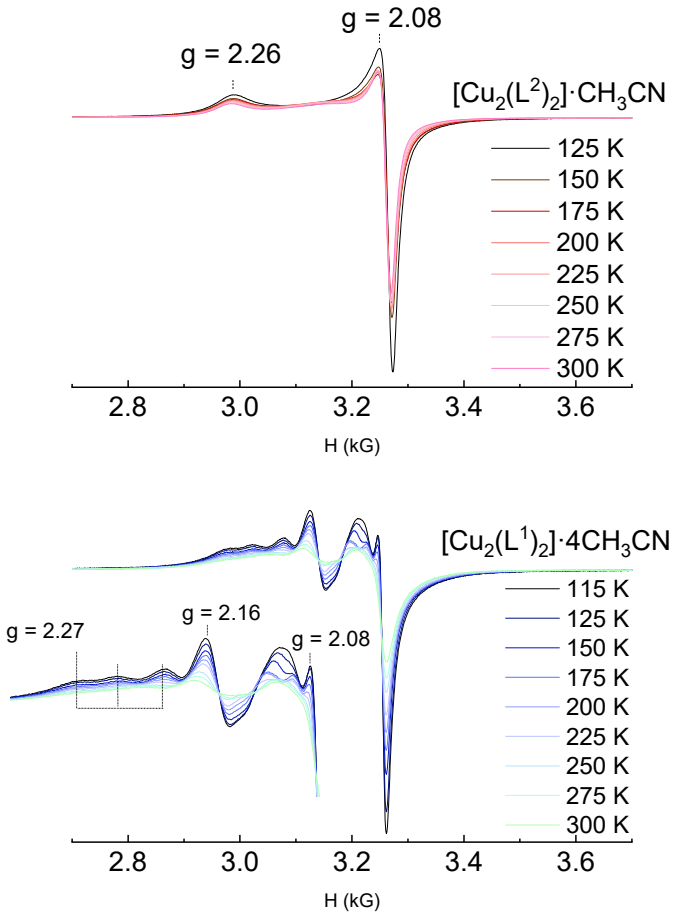

Figure 9. EPR spectra of $[Cu_2(L^2)_2]\cdot CH_3CN$ (top) and $[Cu_2(L^1)_2]\cdot 4CH_3CN$ (bottom) helicates at different temperatures. The inset shows an enlarged portion of the spectrum.

The differences observed in the magnetic behavior of the two reported helicates show that the position of the tert-butyl group in *para* (H_2L^1 ligand) or *ortho* (H_2L^2 ligand) with respect to the phenol group affects to the magnetic behavior of the compounds and, therefore, that the magnetic properties in the helicates can be modulated by small structural changes in the ligands.

3. Materials and Methods

All solvents, 4,4'-methylenedianiline, 3-tert-butyl-2-hydroxybenzaldehyde, 5-tert-butyl-2-hydroxybenzaldehyde and copper plates were purchased from commercial sources and were used without purification. Melting points were determined using a BUCHI 560 instrument. Elemental analysis of compounds (C, N and H) were carried out on a FISONS EA model 1108 analyzer. Infrared spectra were recorded from 4000 to 500 cm-1 on a BRUKER FT-MIR spectrophotometer model VERTEX 70V in solid state using KBr pellets. Mass spectra were obtained using Bruker Microtof spectrometers for the ESI+ technique (electrospray ionization in positive mode) and Bruker Autoflex for the MALDI technique (matrix assisted laser desorption/ionization), both coupled to a time-of-flight (TOF) analyzer. A Varian Inova 400 spectrometer was employed to record the ^1H NMR spectra operating at room temperature using acetone-d_6 as deuterated solvent. Chemical shifts are reported as δ (in ppm).

4.1. Synthesis and characterization of the Schiff base ligands H_2L^1 and H_2L^2

H_2L^1: 0.5 g (2.5 mmol) of 4,4'-methylenedianiline and 0.88 mL (5.0 mmol) of 5-tert-butyl-2-hydroxybenzaldehyde were dissolved in absolute ethanol (50 mL), adding a catalytic amount of p-toluensulfonic acid. The reaction mixture was heated under reflux with magnetic stirring for 4 h,

Preprints (www.preprints.org) | NOT PEER-REVIEWED | Posted: 28 April 2023 doi:10.20944/preprints202304.1135.v1

using a Dean-Stark manifold to remove water and promote ligand formation. The resulting solution was concentrated to half volume and cooled, resulting in the formation of an orange precipitate. This solid was filtered and air-dried. Yield: 0.914 g (70%); m.p.: 155-160 °C; elemental analysis: % theoretical ($C_{35}H_{38}N_2O_2$) C, 81.0; N, 5.4; H, 7.4; experimental C, 81.4; N, 5.4; H, 7.3; IR (cm^{-1}) ν: 3443 w (O-H); 2957 s (C-H); 1622 s (C=N); 1265 m (C-O); 820 vs (CH_2); ESI+ (m/z): 519.30 $[H_2L^1+H]^+$; ^{1}H-NMR (400 MHz, acetone-d_6, δ (m, nH, Hx, J)): 12.98 (s, 2H, H_1), 8.92 (s, 2H, H_2), 7.91 (d, J= 2.5 Hz, 2H, H_3); 7.47 (dd, J= 8.7, 2.5 Hz, 2H, H_4), 7.37 (s, 8H, H_5+H_6); 6.89 (d, J= 8.7 Hz, 2H, H_7); 4.08 (s, 2H, H_8), 1.32 (s, 18H, H_9).

H_2L^2: 0.5 g (2.5 mmol) of 4,4'-methylenedianiline and 0.88 mL (5.0 mmol) of 3-tert-butyl-2-hydroxybenzaldehyde were dissolved in absolute ethanol (50 mL). Then, a catalytic amount of p-toluensulphonic acid was added and the reaction mixture was heated under reflux with magnetic stirring for 4 h, using a Dean-Stark manifold to remove water and promote ligand formation. The resulting solution was concentrated to half volume and cooled resulting in the formation of a yellow precipitate. This solid was filtered and dried in air Yield: 1.02 g (78%); m.p.: 105-110 °C; elemental analysis: % theoretical ($C_{35}H_{38}N_2O_2$) C, 81.0; N, 5.4; H, 7.4; experimental C, 80.8; N, 5.4; H, 7.2; IR (cm^{-1}) ν: 3437 vw (O-H); 2955 s (C-H); 1616 vs (C=N); 1277 m (C-O); 745 s (CH_2); ESI+ (m/z): 519.30 $[H_2L^2+H]^+$; ^{1}H-NMR (400 MHz, acetone-d_6, δ (m, nH, Hx, J)): 14.01 (s, 2H, H_1), 8.90 (s, 2H, H_2), 7.44-7.37 (m, 12H, H_3-H_6); 6.89 (t, J= 7 Hz, 2H, H_7); 4.09 (s, 2H, H_8), 1.44 (s, 18H, H_9).

4.2. Synthesis and characterization of the neutral copper(II) dihelicates

The neutral copper(II) helicates were obtained by electrochemical synthesis using acetonitrile as solvent, applying a current intensity of 10 mA and potential values in the interval of 10-15 V. As example, we describe below the electrochemical synthesis of the $[Cu_2(L^1)_2]$ helicate:

The electrochemical cell can be denoted as Pt(-) | H_2L^1+ CH_3CN | Cu(+). The H_2L^1 ligand (0.05 g, 0.10 mmol) was previously dissolved in acetonitrile (80 mL) and a small amount of tetraethylammonium perchlorate was added to act as a conducting electrolyte. The electrolytic reaction was carried out under N_2(g) atmosphere at 10 mA and 13.0 V for 31 min. The resulting solution was concentrated, giving rise to a brown solid that was filtered off and dried in vacuo. Caution! Although perchlorate salts were used in very small quantities in these reactions, they are potentially explosive and should be used with care.

The main analytical and characterization data of both copper(II) complexes are given below.

$[Cu_2(L^1)_2]$: Brown solid. Yield: 0.068 g (61%); m.p.: > 300 °C; Ef = 0.6 mol·F^{-1}; elemental analysis: % theoretical ($C_{70}H_{72}N_4O_4Cu_2$) C, 72.5; N, 4.8; H, 6.2; experimental C, 70.9; N, 4.8; H, 6.2; IR (cm^{-1}) ν: 3397 br (O-H); 2954 m (C-H); 1618 vs (C=N); 1255 m (C-O); 833 s (CH_2); MALDI-TOF (m/z): 1159.42 $[Cu_2(L^1)_2+H]^+$. By slow evaporation of the mother liquor from the synthesis, brown crystals suitable for X-ray diffraction studies were obtained ($[Cu_2(L^1)_2]\cdot 4CH_3CN$).

$[Cu_2(L^2)_2]\cdot CH_3CN$: Brown solid. Yield: 0.079 g (68%); m.p.: > 300 °C; Ef = 0.5 mol·F^{-1}; elemental analysis: % theoretical ($C_{72}H_{75}N_5O_4Cu_2$) C, 72.0; N, 5.8; H, 6.3; experimental C, 71.5; N, 5.3; H, 6.2; IR (cm^{-1}) ν: 2953 m (C-H); 1611 s (C=N); 1246 w (C-O); 750 s (CH_2); MALDI-TOF (m/z): 1159.42 $[Cu_2(L^2)_2+H]^+$. By slow evaporation of the mother liquor from the synthesis, brown crystals suitable for X-ray diffraction studies were obtained ($[Cu_2(L^2)_2]\cdot CH_3CN$).

4.3. X-ray Crystallography

Crystallographic data for both copper(II) dihelicates ($[Cu_2(L^1)_2]\cdot 4CH_3CN$) and ($[Cu_2(L^2)_2]\cdot CH_3CN$) were collected at 100 K on a Bruker D8 VENTURE diffractometer equipped with a CCD detector, using a MoK (α) graphite monochromator (λ = 0.71073 Å). The data were treated with APPEX3v2018.7-2 software for both compounds.

In all cases, an absorption correction (SADABS) [34] was applied to the measured reflections. Structures were solved with SHELXT2018/2 [35]. All structures were refined using SHELXL2018/3 [35]. The hydrogen atoms were included in the model in geometrically calculated and refined positions. The images included in this chapter were prepared using Mercury [36]. CCDC no. 2257783

and 2257784 contains the supplementary crystallographic data for the $[Cu_2(L^1)_2]\cdot 4CH_3CN$ and $[Cu_2(L^1)_2]\cdot CH_3CN$ dihelicates.

4.4. EPR spectroscopy

EPR spectra of both copper(II) helicates $[Cu_2(L^1)_2]\cdot 4CH_3CN$ and $[Cu_2(L^2)_2]\cdot CH_3CN$ were recorded at different temperatures using a Bruker EMX spectrometer operating at 9.5 GHz (X-Band).

4.5. Magnetic susceptibility measurements

DC magnetic susceptibility measurements for microcrystalline copper(II) helicates were performed at different fields in a MPMS SQUID magnetometer from Quantum Design, from 5-300 K.

5. Conclusions

Two novel Cu(II) neutral dinuclear helicates were isolated using an electrochemical methodology and precursor Schiff base ligands functionalized with bulky tert-butyl groups in *ortho* and *para* positions. The discrete crystal structures of both copper(II) compounds $[Cu_2(L^1)_2]\cdot 4CH_3CN$ and $[Cu_2(L^1)_2]\cdot CH_3CN$ confirm their helicoidal dinuclear nature. These structures are extended through the establishment of weak π-π or CH····π stacking interactions, being the intermolecular metal distance smaller than the distance between the metal ions within the molecule, especially in the case of $[Cu_2(L^1)_2]\cdot 4CH_3CN$ with the external tert-butyl groups located far away from the binding domains, thus confirming the influence of the bulky group location. This structural fact also influences the magnetic properties of the helicates in terms of local environments of the Cu(II) ions, but this finding will require further studies.

Supplementary Materials: The following supporting information can be downloaded at the website of this paper posted on Preprints.org, Figure S1: ^1H NMR spectra of H_2L^1 (400 MHz, acetone-d_6, r.t., δ (m, nH, Hx, J)); Figure S2: ^1H NMR spectra of H_2L^2 (400 MHz, acetone-d_6, r.t., δ (m, nH, Hx, J)); Figure S3: Infrared spectra superposition of H_2L^1 (pink) and $[Cu_2(L^1)_2]$ (blue); Figure S4: Intermolecular CH···π interactions in the crystal lattice of the $[Cu_2(L^1)_2]\cdot 4CH_3CN$ helicate; Figure S5: Intermolecular π ···π interactions in the crystal lattice of the $[Cu_2(L^2)_2]\cdot CH_3CN$ helicate); Table S1: Main crystallographic data for helicates $[Cu_2(L^1)_2]\cdot 4CH_3CN$ and $[Cu_2(L^2)_2]\cdot CH_3CN$; Table S2: Main bond distances and angles for $[Cu_2(L^1)_2]\cdot 4CH_3CN$ helicate; Table S3: Main bond distances and angles for $[Cu_2(L^2)_2]\cdot CH_3CN$ helicate.

Author Contributions: Conceptualization, S.F.-F., M. M., A.M.G.-N. and R.P.; methodology, S.F.-F., M.M.-C., I. V.-H, F. R., A.M.G.-N. and R.P.; formal analysis, S.F.-F.; investigation, S.F.-F., I. V.-H , M.M.-C., , M. M, F. R., A.M.G.-N and R.P.; resources, A.M.G.-N., R.P. and M.M.; data curation, S.F.-F., I.V.-H., F. R..; writing—original draft preparation, S.F.-F., I.V.-H., M.M., F. R. , A.M.G.-N and R.P.; writing—review and editing, S.F.-F., F. R., A.M.G.-N and R.P.; supervision, A.M.G.-N. and R.P.; project administration, M. M, A.M.G.-N. and R.P.; funding acquisition, M. M. A.M.G.-N. and R.P. All authors have read and agreed to the published version of the manuscript.".

Funding: This research was funded by the following FEDER co-funded grants. From Consellería de Cultura, Educación e Ordenación Universitaria, Xunta de Galicia, 2017GRCGI-1682 (ED431C2017/01), 2018GRCGI-1584 (ED431C2018/13), MetalBIONetwork (ED431D2017/01). From Ministerio de Ciencia, Innovación y Universidades, METALBIO (CTQ2017-90802-REDT). From Ministerio de Ciencia e Innovación, MultiMetDRUGS (RED2018-102471-T) and Project PID2021-127531NB-I00 (AEI/10.13039/501100011033/ FEDER, UE).

Institutional Review Board Statement: Not applicable.

Data Availability Statement: Crystallographic data for $[Cu_2(L^1)_2]\cdot 4CH_3CN$ and $[Cu_2(L^2)_2]\cdot CH_3CN$ were deposited into the Cambridge Crystallographic Data Centre, CCDC 2257783 and 2257784. These data can be obtained free of charge via www.ccdc.cam.ac.uk/data_request/cif, or by emailing data_request@ccdc.cam.ac.uk, or by contacting The Cambridge Crystallographic Data Centre, 12 Union Road, Cambridge CB2 1EZ, UK; fax: +44 1223 336033.

Conflicts of Interest: The authors declare no conflict of interest.

References

1. Fernández-Fariña, S.; Martínez-Calvo, M.; Maneiro, M.; Seco, J. M.; Zaragoza, G.; González-Noya, A. M.; Pedrido, R. Two Synthetic Approaches to Coinage Metal(I) Mesocates: Electrochemical versus Chemical Synthesis. *Inorg. Chem.* **2022**, *61* (35), 14121–14130.
2. Lehn, J. M.; Rigault, A.; Siegel, J.; Harrowfield, J.; Chevrier, B.; Moras, D. Spontaneous Assembly of Double-Stranded Helicates from Oligobipyridine Ligands and Copper(I) Cations: Structure of an Inorganic Double Helix. *Proc. Natl. Acad. Sci. U. S. A.* **1987**, *84* (9), 2565–2569.
3. McTernan, C. T.; Ronson, T. K.; Nitschke, J. R. Selective Anion Binding Drives the Formation of $Ag^{I}_{8}L_{6}$ and $Ag^{I}_{12}L_{6}$ Six-Stranded Helicates. *J. Am. Chem. Soc.* **2021**, *143* (2), 664–670.
4. Hannon, M. J.; Childs, L. J. Helices and Helicates: Beautiful Supramolecular Motifs with Emerging Applications. *Supramol. Chem.* **2004**, *16* (1), 7–22.
5. Albrecht, M. "Let's Twist Again" - Double-Stranded, Triple-Stranded, and Circular Helicates. *Chem. Rev.* **2001**, *101* (11), 3457–3497.
6. Piguet, C.; Bernardinelli, G.; Hopfgartner, G. Helicates as Versatile Supramolecular Complexes. *Chem. Rev.* **1997**, *97* (6), 2005–2062.
7. Cooke, D. J.; Cross, J. M.; Fennessy, R. V.; Harding, L. P.; Rice, C. R.; Slater, C. Steric Control of the Formation of Dinuclear Double Helicate and Dinuclear Meso -Helicate Assemblies. *Chem. Commun.* **2013**, *49* (71), 7785–7787.
8. Ronson, T. K.; Adams, H.; Riis-Johannessen, T.; Jeffery, J. C.; Ward, M. D. Mixed Ligand Helicates and Mesocates. *New J. Chem.* **2006**, *30* (1), 26–28.
9. Mayans, J.; Font-Bardia, M.; Di Bari, L.; Arrico, L.; Zinna, F.; Pescitelli, G.; Escuer, A. From Mesocates to Helicates: Structural, Magnetic and Chiro-Optical Studies on Nickel(II) Supramolecular Assemblies Derived from Tetradentate Schiff Bases. *Chem. Eur. J.* **2018**, *24* (30), 7653–7663.
10. Fernández-Fariña, S.; Velo-Heleno, I.; Martínez-Calvo, M.; Barcia, R.; Palacios, Ò.; Capdevila, M.; González-Noya, A. M.; Pedrido, R. Exploring the Biological Properties of Zn (II) Bis Thiosemicarbazone Helicates. *Int. J. Mol. Sci.* **2023**, *24*, 2246.
11. Ono, T.; Ishihama, K.; Taema, A.; Harada, T.; Furusho, K.; Hasegawa, M.; Nojima, Y.; Abe, M.; Hisaeda, Y. Dinuclear Triple-Stranded Helicates Composed of Tetradentate Ligands with Aluminum(III) Chromophores: Optical Resolution and Multi-Color Circularly Polarized Luminescence Properties. *Angew. Chem. Int. Ed.* **2021**, *60* (5), 2614–2618.
12. Craen, D. Van; Kalarikkal, M. G.; Holstein, J. J. A Charge-Neutral Self-Assembled L 2 Zn 2 Helicate as Bench-Stable Receptor for Anion Recognition at Nanomolar Concentration. *J. Am. Chem. Soc.* **2022**, *144*, 18135–18143.
13. Gunnlaugsson, T.; Hegarty, I.; Barry, D.; Byrne, J. P.; Kotova, O. Formation of Lanthanide Luminescent Di-Metallic Helicates in Solution Using a Bis-Tridentate (1,2,3-Triazol-4-Yl)-Picolinamide (Tzpa) Ligand. *Chem. Commun.* **2023, Accepted Manuscript**.(DOI: 10.1039/D3CC01126G)
14. Kalinke, L. H. G.; Rabelo, R.; Valdo, A. K.; Martins, F. T.; Ferrando-soria, J.; Julve, M.; Lloret, F.; Cano, J.; Cangussu, D. Trinuclear Cobalt(II) Triple Helicate with a Multidentate Bithiazolebis(Oxamate) Ligand as a Supramolecular Nanomagnet. *Inorg. Chem.* **2022**, *61*, 5696–5700.
15. Diego, R.; Pavlov, A.; Darawsheh, M.; Aleshin, D.; Nehrkorn, J.; Nelyubina, Y.; Roubeau, O.; Novikov, V.; Aromí, G. Coordination [CoII2] and [CoIIZnII] Helicates Showing Slow Magnetic Relaxation. *Inorg. Chem.* **2019**, *58* (15), 9562–9566.
16. Gao, X.; Li, L.; Sun, W.; Chen, P. Crystallization and Single Molecule Magnetic Behavior of Quadruple-Stranded Helicates: Tuning the Anisotropic Axes. *Dalton Trans.* **2020**, *49* (9), 2843–2849.
17. Fabbrizzi, L. Beauty in Chemistry: Making Artistic Molecules with Schiff Bases. *J. Org. Chem.* **2020**, *85* (19), 12212–12226.
18. Wang, Z.; Zhou, L. P.; Cai, L. X.; Tian, C. Bin; Sun, Q. F. From a Mononuclear FeL_2 Complex to a Fe_4L_4 Molecular Square: Designed Assembly and Spin-Crossover Property. *Nano Res.* **2021**, *14* (2), 398–403.
19. Wang, Y. T.; Li, S. T.; Wu, S. Q.; Cui, A. L.; Shen, D. Z.; Kou, H. Z. Spin Transitions in Fe(II) Metallogrids Modulated by Substituents, Counteranions, and Solvents. *J. Am. Chem. Soc.* **2013**, *135* (16), 5942–5945.
20. Escuer, A. A.; Mayans, J.; Bari, L. Di; Font-, M.; Arrico, L.; Zinna, F. From Mesocates to Helicates: Nickel(II) Supramolecular Assemblies Derived from Tetradentate Schiff Bases. Structural, Magnetic and Chiro-Optical Studies. *Chem. Eur. J.* **2018**, *24*, 7653–7663.
21. Hrabina, O.; Malina, J.; Kostrhunova, H.; Novohradsky, V.; Pracharova, J.; Rogers, N.; Simpson, D. H.; Scott, P.; Brabec, V. Optically Pure Metallohelices That Accumulate in Cell Nuclei, Condense/Aggregate DNA, and Inhibit Activities of DNA Processing Enzymes. *Inorg. Chem.* **2020**, *59* (5), 3304–3311.
22. Vázquez, M.; Taglietti, A.; Gatteschi, D.; Sorace, L.; Sangregorio, C.; González, A. M.; Maneiro, M.; Pedrido, R. M.; Bermejo, M. R. A 3D Network of Helicates Fully Assembled by π-Stacking Interactions. *Chem. Commun.* **2003**, *3* (15), 1840–1841.
23. Hooper, C. A. J.; Cardo, L.; Craig, J. S.; Melidis, L.; Garai, A.; Egan, R. T.; Sadovnikova, V.; Burkert, F.; Male, L.; Hodges, N. J.; Browning, D. F.; Rosas, R.; Liu, F.; Rocha, F. V; Lima, M. A.; Liu, S.; Bardelang, D.; Hannon,

M. J. Rotaxanating Metallo-Supramolecular Nano-Cylinder Helicates to Switch DNA Junction Binding. *J. Am. Chem. Soc.* **2020**, *142*, 20651–20660.
24. Malina, J.; Hannon, M. J.; Brabec, V. Iron(II) Supramolecular Helicates Condense Plasmid DNA and Inhibit Vital DNA-Related Enzymatic Activities. *Chem. Eur. J.* **2015**, *21* (31), 11189–11195.
25. Cardo, L.; Nawroth, I.; Cail, P. J.; McKeating, J. A.; Hannon, M. J. Metallo Supramolecular Cylinders Inhibit HIV-1 TAR-TAT Complex Formation and Viral Replication in Cellulo. *Sci. Rep.* **2018**, *8* (1), 2–8.
26. Yusuf, T. L.; Oladipo, S. D.; Zamisa, S.; Kumalo, H. M.; Lawal, I. A.; Lawal, M. M.; Mabuba, N. Design of New Schi Ff -Base Copper (II) Complexes : Synthesis , Crystal Structures , DFT Study , and Binding Potency toward Cytochrome. *ACS Omega* **2021**, *6*, 13704–13718.
27. Wallis, M. J.; Min, H.; Lindoy, L. F.; Li, F. Investigating the Conformations of a Family of $[M_2L_3]^{4+}$ Helicates Using Single Crystal X-Ray Diffraction. *Molecules* **2023**, *28*, 1404.
28. G. A. Jeffrey. *An Introduction to Hydrogen Bonding, Oxford University Press*; 1997.
29. Cucos, P.; Tuna, F.; Sorace, L.; Matei, I.; Maxim, C.; Shova, S.; Gheorghe, R.; Caneschi, A.; Hillebrand, M.; Andruh, M. Magnetic and Luminescent Binuclear Double-Stranded Helicates. *Inorg. Chem.* **2014**, *53* (14), 7738–7747.
30. Pedrido, R.; Vázquez López, M.; Sorace, L.; González-Noya, A. M.; Cwiklinska, M.; Suárez-Gómez, V.; Zaragoza, G.; Bermejo, M. R. The Coordination Preferences of Metal Centres Modulate Superexchange Coupling Interactions in a Metallo-Supramolecular Helical Assembly. *Chem. Commun.* **2010**, *46* (26), 4797–4799.
31. Palacios, M. A.; Díaz-Ortega, I. F.; Nojiri, H.; Suturina, E. A.; Ozerov, M.; Krzystek, J.; Colacio, E. Tuning Magnetic Anisotropy by the π-Bonding Features of the Axial Ligands and the Electronic Effects of Gold(i) Atoms in 2D {Co(L)2[Au(CN)2]2}: Nmetal-Organic Frameworks with Field-Induced Single-Ion Magnet Behaviour. *Inorg. Chem. Front.* **2020**, *7* (23), 4611–4630.
32. Peisach, J.; Blumberg, W. E. Structural Implications Derived from the Analysis Resonance Spectra of Natural of Electron and Paramagnetic Artificial. *Arch. Biochem. Biophys.* **1974**, *165*, 691–708.
33. Seebauer, E. G.; Buliba, E. P.; Scogin, D. A.; Gennis, R. B.; Belford, R. L. EPR Evidence on the Structure of the Copper(II)-Bacitracin A Complex. *JACS* **1983**, *105*, 4926–4929.
34. Sheldrick, G. M. *Program for Scaling and Correction of Area Detector Data*, University.; 1996.
35. Sheldrick, G. M. Crystal Structure Refinement with SHELXL. *Acta Crystallogr.* **2015**, *C71*, 3–8.
36. Macrae, C. F.; Bruno, I. J.; Chisholm, J. A.; Edgington, P. R.; Mccabe, P.; Pidcock, E.; Rodriguez-monge, L.; Taylor, R.; Streek, J. Van De; Wood, P. A. Mercury CSD 2 . 0 – New Features for the Visualization and Investigation of Crystal Structures. *J. Appl. Crystallogr.* **2008**, 466–470.